Progress in Nuclear Energy 188 (2025) 105876

Contents lists available at ScienceDirect

Progress in Nuclear Energy

journal homepage: www.elsevier.com/locate/pnucene

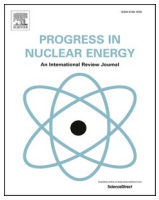

Multi-physics multi-scale thermal-hydraulic analysis of the steam line break accident for the SMART small modular reactor with TRACE/PARCS/OpenFOAM

Kanglong Zhang *, Victor Hugo Sanchez-Espinoza

Karlsruhe Institute of Technology (KIT), Hermann-von-Helmholtz-Platz 1, Eggenstein-Leopoldshafen, 76344, Germany

ARTICLE INFO

Keywords:
Multi-physics
Multi-scale
SMART
Steam line break
TRACE/PARCS/OpenFOAM

ABSTRACT

Within the framework of the EU McSAFER project, advanced multi-physics and multi-scale thermal-hydraulic codes have been developed and validated for the safety analysis of innovative Small Modular Reactors (SMRs). This paper concentrates on modeling and analyzing a Steam Line Break (SLB) accident for the SMART reactor using the coupling code TRACE/PARCS/OpenFOAM developed at KIT. Specifically, OpenFOAM is employed to describe the flow characteristics within the downcomer and lower plenum, while TRACE simulates the Thermal-Hydraulic (TH) phenomena in other regions of the reactor pressure vessel (RPV) as well as in the steam lines and passive heat removal system. PARCS is utilized for core neutronics simulations. Starting from normal operating conditions, a double-ended break in one of the eight steam lines, resulted in a sudden pressure drop within that tube consequently triggering a SCRAM signal. In addition, a coincident loss of offsite power is assumed that leads to the coast-down of the four main pumps. Throughout this transient event, the coupled code successfully predicts global phenomena, such as the transition from forced convection to natural convection within the reactor vessel, thereby validating the inherent passive safety features of the SMART reactor. Moreover, the couple code is able to capture the three-dimensional asymmetrical coolant mixing in the downcomer, lower plenum, and its impact on the core behavior in great detail.

1. Introduction

The Small Modular Reactor (SMR) is characterized by low-power, modularization employed throughout its design, construction, and deployment phases (International Atomic Energy Agency, 2021). Numerous innovative technologies have been developed for SMRs, as defined by the International Atomic Energy Agency (IAEA) (International Atomic Energy Agency, 1997), including the compact Reactor Pressure Vessel (RPV) and passive decay heat removal systems, to enhance their safety. These features make SMRs an attractive option for different applications in addition to electricity generation such as heat, hydrogen, and water desalination. Many SMRs are currently under development worldwide, with the most widely recognized being SMART (Kamalpour and Khalafi, 2021), NuScale (Sadegh-Noedoost et al., 2020), and CAREM (Tashakor et al., 2017).

Upon the design and manufacturing of SMRs, licensing becomes the decisive factor for final deployment. Therefore, safety analysis and evaluation must be performed for SMRs. Among various phenomena that can occur in SMRs, the asymmetrical behavior during accidents, such as Steam Line Break (SLB), boron dilution, and control rod ejection, must be analyzed. This requirement primarily stems from the licensing experience of large Pressurized Water Reactors (PWRs), although the circumstances differ for SMRs. For example, typical large PWRs, such as those with a two-loop configuration, may experience re-criticality and unsymmetrical power increases during undercooling transients like SLB. The impact of these phenomena decreases with an increasing number of loops, which is typical for water-cooled SMRs. Consequently, it is of significant interest to investigate the SLB accident in water-cooled SMRs with integrated RPVs, where the Steam Generators (SGs) are located inside the RPV, and additional devices are designed and placed around the core to promote primary coolant mixing, as in the SMART reactor.

To validate these phenomena and the relevant safety structures, a wide array of studies, including experiments and simulations, are conducted. Among these, the use of advanced simulation methods, such as multi-physics and multi-scale Thermal-Hydraulic (TH) tools, is increasingly prevalent. The multi-physics and multi-scale TH methods

* Corresponding author.
E-mail addresses: kanglong.zhang2@kit.edu (K. Zhang), victor.sanchez@kit.edu (V.H. Sanchez-Espinoza).

https://doi.org/10.1016/j.pnucene.2025.105876
Received 4 December 2024; Received in revised form 12 May 2025; Accepted 5 June 2025
Available online 7 June 2025

were first developed and applied to the safety analysis of traditional large nuclear power plants. Recent activities include the development and validation of coupling codes such as TRACE/PARCS (Watson and Ivanov, 2012), COBAYA3/SubChanFlow(SCF) (Calleja et al., 2014), and TRACE/SCF (Zhang et al., 2021). A comprehensive review of these coupling activities from a multi-scale TH perspective is provided in (Zhang, 2020).

In this research field, the Karlsruhe Institute of Technology (KIT) has launched the EU project McSAFER (Sanchez-Espinoza et al., 2021) to explore safety analyses for SMRs employing advanced multi-physics and multi-scale TH methods and perform experimental investigations. Within the project's scope, KIT has developed a generic multi-physics and multi-scale TH coupling platform incorporating the system TH code TRACE, the sub-channel code SubChanFlow (SCF), the porous media code TwoPorFlow (TPF), the CFD code OpenFOAM, the deterministic core neutronic code PARCS, and the Monte Carlo neutronic code Serpent (Hugo Sanchez-Espinoza et al., 2023) (Sanchez-Espinoza et al., 2023), facilitating both normal and high-fidelity safety analyses of SMRs. This platform is highly standardized, modularized, and extensible. Codes in this platform could be flexibly coupled according to specific problems. Moreover, advanced techniques, e.g., relaxation, acceleration, are developed to enhance the coupling efficiency and robustness.

This paper examines the safety analysis of the SMART reactor during the SLB accident using the multi-physics and multi-scale TH coupling code TRACE/PARCS/OpenFOAM. It begins with an introduction to the codes, coupling methodologies, and the coupling code itself. Subsequently, the SMART reactor and the corresponding models of these codes are delineated, followed by a discussion of the SLB transient and the resulting findings.

2. The codes and coupling methodology

This section provides an overview of the codes comprising both the coupling system and the individual components, along with the methodologies employed for their integration.

2.1. TRACE(Bajorek et al., 2015)

The TRACE is a system thermal-hydraulic code developed by the U.S. Nuclear Regulatory Commission (NRC) for performing transient analyses in Light Water Reactors (LWRs). It can operate using either an integrated point kinetics model or the 3D nodal diffusion solver PARCS, which is coupled with TRACE for enhanced neutronic-thermal hydraulic interactions. TRACE solves six conservation equations—covering mass, momentum, and energy balances—for two-phase flows in 1D and 3D geometry. These capabilities are supported by a variety of detailed heat transfer and flow regime models that span the entire boiling curve, accommodating both vertical and horizontal flow orientations.

For the numerical resolution of its governing equations, TRACE incorporates constitutive models that account for heat and mass transfer at solid-fluid interfaces, along with frictional effects at both the wall and interface. Its modular design allows users to simulate a wide array of reactor components, such as piping systems, pressurizers, pumps, heat exchangers, steam generators, valves, and even complex containment structures. The code also includes control systems for simulating operator-initiated or automated reactor control actions, such as valve operations, pump shutdowns, or control rod movements, further enhancing its capabilities in transient and accident scenario analysis.

Although TRACE employs a coarse spatial grid for system-wide modeling efficiency, which may reduce the granularity of TH predictions, particularly within the reactor core, it compensates for this with a dedicated 3D Cartesian model for core TH analysis. However, this core model lacks the fine resolution offered by sub-channel codes, which are capable of predicting localized safety metrics, such as the Departure from Nucleate Boiling Ratio (DNBR), at the pin or sub-channel level. This makes TRACE more suited for broad system performance assessments rather than highly localized safety parameter predictions.

2.2. PARCS (Downar et al., 2012)

PARCS, developed by the U.S. NRC, is a 3D reactor core simulator that solves steady-state eigenvalue problems as well as time-dependent neutron diffusion and low-order transport equations. It is versatile in terms of geometry, supporting both Cartesian and hexagonal meshes. To handle time discretization, PARCS uses the theta method with an exponential transformation, combined with a second-order analytic precursor integration technique, enabling the use of large time steps while maintaining accuracy.

For spatial discretization, PARCS employs the efficient coarse mesh finite difference method, supplemented by advanced two-node solvers like the nodal expansion method and the analytic nodal method for Cartesian geometries at the fuel assembly level. For hexagonal meshes, a dedicated triangular polynomial expansion method is used. Additionally, when fine spatial resolution is required, PARCS can perform pin-level calculations using a fine mesh finite difference solver.

To incorporate TH feedback into its neutron kinetics simulations, PARCS includes a module known as the PARCS Advanced Thermal Hydraulic Solver (PATHS). While PATHS provides simplified thermal-hydraulic feedback, it uses a decoupled approach to solve velocity and pressure equations. As a result, although it is suitable for general core-wide thermal-hydraulic analysis, it may not provide the level of detail required for more localized or fine-scale thermal-hydraulic phenomena, such as those addressed by specialized sub-channel codes.

2.3. OpenFOAM (OpenFOAM Foundation)

OpenFOAM is a open-source Computational Fluid Dynamics (CFD) platforms. It serves as a highly flexible framework for developing custom application executables, built upon a robust collection of around 100 C++ libraries. With approximately 250 pre-built applications, OpenFOAM categorizes them into two main types: solvers, designed to address specific problems in fluid dynamics and continuum mechanics, and utilities, which are primarily used for data manipulation, mesh handling, and post-processing. One of the key strengths of OpenFOAM is its extensibility. Users are free to expand its capabilities by creating additional solvers, utilities, and libraries, as long as they possess a solid understanding of the underlying physics, numerical methods, and programming techniques. This flexibility makes OpenFOAM suitable for a wide variety of CFD applications, from academic research to industrial use. OpenFOAM also integrates pre-processing and post-processing tools into its framework, with these tools themselves treated as utilities within the platform. This design choice ensures consistency and smooth data management throughout all stages of a simulation, from setting up initial conditions to analyzing results.

However, applying CFD codes like OpenFOAM to nuclear safety analysis poses significant challenges. First, there is the issue of high computational cost, particularly when large-scale systems, such as complete Nuclear Power Plants (NPPs), need to be modeled. Simulating the complex dynamics of such systems often requires immense computational resources. Second, accurately resolving two-phase flow phenomena—critical in NPPs—is particularly difficult. Two-phase flows involve complex interactions between liquid and gas phases and are essential for simulating key processes like boiling and condensation, which are fundamental to the safety and operation of nuclear reactors.

2.4. The coupled code TRACE/PARCS/OpenFOAM

As indicated, the three codes were integrated within a generic multi-physics and multi-scale Thermal-Hydraulic (TH) platform. Each of these codes was furnished with an ICoCo interface, which stands for Interface for Code Coupling (SALOME Platforma). This interface serves as a

modularized standard that delineates methods for encapsulating the code to be integrated into C++ classes, where the code's native functions are transformed into the classes' methods. A C++ supervisor orchestrates the interaction among the coupled codes and facilitates inter-code data transfer through the ICoCo interfaces. The foundational structure of this coupling system is illustrated in Fig. 1.

According to the coupling categories and methods outlined in (Zhang, 2020), the specific technical features of this coupling code are as follows.

1) Parallel running: The implementation of the Message Passing Interface (MPI) is primarily aimed at accelerating the OpenFOAM simulations and the execution of all coupled codes.
2) External coupling: The codes, along with their respective ICoCo interfaces, are encapsulated from each other, with interactions facilitated solely through the supervisor.
3) Domain-decomposition coupling: TRACE and OpenFOAM assume responsibility for distinct Thermal-Hydraulic (TH) domains, with OpenFOAM simulating the downcomer and lower plenum, while TRACE is tasked with modeling the core and upper plenum.
4) Automatic field translation: Inter-code communication occurs through the transmission of new time solutions, with the MEDCoupling library (SALOME Platformb) employed to automatically translate fields with varying dimensions and meshes.
5) Explicit coupling: Also known as the operator-splitting method, inter-code data communication takes place only once within each time step, with no assurance of convergence for the transferred data. It should be noted that some more advanced methods e.g., the Jacobian-Free Neuton-Krylov (JFNK) method (Zhang et al., 2018), (Liu et al., 2024) which improve the numerical stability of the temporal coupling and might be implemented to the coupled codes shown in this paper.

The first two points are centered on computer science perspectives, while the latter three points are grounded in physical considerations. Additionally, the first, second, and fifth points primarily pertain to the operational procedures of the coupled code. The procedural logic aligns closely with previous works developed at KIT, such as TRACE/Subchanflow-ICoCo (Zhang et al., 2021), TRACE/TrioCFD-ICoCo (Zhang et al., 2020a), and Subchanflow/TrioCFD-ICoCo (Zhang et al., 2020b). The flowcharts presented in these papers serve as valuable references.

Furthermore, the second point delineates the domain allocation of the coupled code. In this instance, OpenFOAM is responsible for TH simulations in the downcomer and lower plenum, TRACE handles TH in other sections of the RPV as well as out-vessel structures, while PARCS focuses on core neutronics. Refer to Fig. 2 for a visual representation of this domain allocation.

There exist two interfaces between the three codes.

1) The 2D TH interfaces between TRACE and OpenFOAM, encompass the interface at the downcomer inlet and the interface at the core inlet or lower plenum outlet.
2) The 3D TH-neutronic interface between TRACE and PARCS.

Following the accuracy and stability study conducted for multi-scale

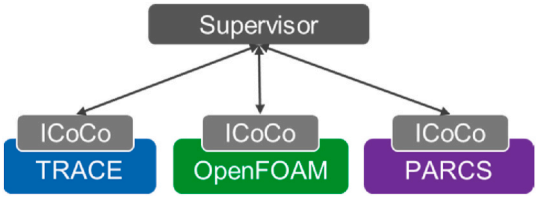

Fig. 1. Overall structure of the coupling code TRACE/PARCS/OpenFOAM.

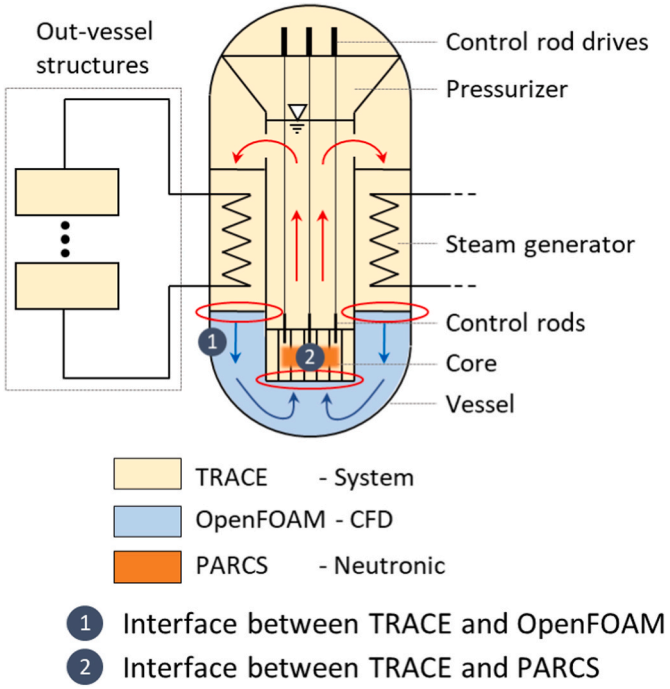

Fig. 2. The domain allocations of the coupled code TRACE/PARCS/OpenFOAM.

TH coupling systems as outlined in (Zhang and Sanchez-Espinoza, 2023), we adopt a conservative data transfer strategy, where the transferred data at the interfaces are as follows.

- Thermal hydraulic coupling for the core inlet (lower plenum outlet) (2D):
  - Pressure (TRACE - > OpenFOAM).
  - Mass flow rate (OpenFOAM - > TRACE).
  - Heat flow rate (mass flow rate times temperature) (OpenFOAM - > TRACE).
- Thermal hydraulic coupling for the downcomer inlet (2D):
  - Pressure (OpenFOAM - > TRACE).
  - Mass flow rate (TRACE - > OpenFOAM).
  - Heat flow rate (mass flow rate times temperature) (trace - > OpenFOAM).
- Neutronic coupling for the core (3D):
  - Power (PARCS - > TRACE).
  - Fuel temperature (TRACE - > PARCS).
  - Coolant temperature (TRACE - > PARCS).
  - Coolant density (TRACE - > PARCS).

To enhance the robustness and efficiency of the coupling simulation, various techniques are implemented within the generic multi-physics and multi-scale TH system, such as the staggered-time-step method. This is a method directly handle the temporal coupling which is the key point affecting the solution stability. With this method, users can specify the time interval to exchange data between the codes, within which, the codes can determine their exact synchronization time point.

3. The SMART reactor and the steam line break (SLB) accident

3.1. The SMART reactor

The integrated modular advanced reactor SMART represents a SMR design developed by the Korea Atomic Energy Research Institute (KAERI) (Chung et al., 2015). This PWR-type SMR generates 330 MW of thermal power, which translates to 100 MW of electricity production.

Notably, its primary coolant system is integrated, housing all primary loop components within the RPV. The power extraction from the RPV is facilitated by eight modular-type, once-through helicoidal SG. Under nominal operating conditions, these generators produce 30 °C superheated steam on the secondary side. Furthermore, the forced-convection flow through the RPV and the core is upheld by four canned pumps. Crucially, the in-vessel pressurizer is engineered to maintain the system pressure at a nearly constant level throughout the design basis events. The core configuration comprises fifty-seven PWR-like fuel assemblies. To ensure a uniform coolant mass flow distribution at the core inlet, a Flow-Mixing Header Assembly (FMHA), and flow skirt are positioned at the SG outlet. Fig. 3 depicts the comprehensive RPV diagram of SMART, showcasing its compact design, aforementioned components, and other key structures within the vessel.

On the secondary side, several auxiliary circuits and safety systems are interconnected with the RPV. Among these, the pressurizer safety valve serves as a primary safety measure, designed to prevent overpressure within the RPV. Another critical safety system is the Passive Residual Heat Removal System (PRHRS), which plays a pivotal role in long-term cooling down the reactor during abnormal shutdown scenarios. Upon activation of the PRHRS, steam from the secondary side is directed towards a large pool, where it undergoes condensation, transforming into water. This condensed water then circulates back to the SG inlet via natural circulation, ensuring effective heat removal from the system. The left of Fig. 4 provides a concise diagram illustrating the operation of the PRHRS. There are four PRHRSs in the SMART reactor, each one of them corresponds to two SGs (total of eight SGs), which are inter-connected via the PRHRS, see right of Fig. 4.

3.2. The steam line break (SLB) accident

Fig. 4 also illustrates the schematic view of some key components e.g., the Feedwater Isolation Valves (FWIVs) and Steam Isolation Valves (SIVs). As the PRHRS, it is composed of an Emergency Cooldown Tank (ECT), four Heat Exchangers (HXs), and one accumulator for each HX, along with connecting pipes and PRHRS Isolation Valves (IVs). In standard operating conditions, the feedwater flows through the FWIVs, enters the RPV, moves through the SGs from the bottom to the top, exits the RPV, passes through the SIVs, and ultimately arrives at the Main Steam Line (MSL). The models utilized in this research treat the feedwater as having a constant inlet mass flow rate, while the turbine maintains a fixed outlet pressure.

In this safety analysis, the scenario of an SLB is modeled to occur in the steam line of SG1, specifically considering a double-ended guillotine break. The water inventory released due to this incident is sourced from both SG1 and SG2 since SG2 is interconnected with SG1 via the PRHRS. Under normal operating conditions, the FWIVs and SIVs remain open, whereas the PRHRS IVs are kept closed. The primary focus of this analysis is to evaluate the potential for a significant return to power and re-criticality, despite the reactor being in a shutdown state, resulting from positive reactivity insertion due to the cooling of the primary coolant, a common occurrence in large Pressurized Water Reactors (PWRs).

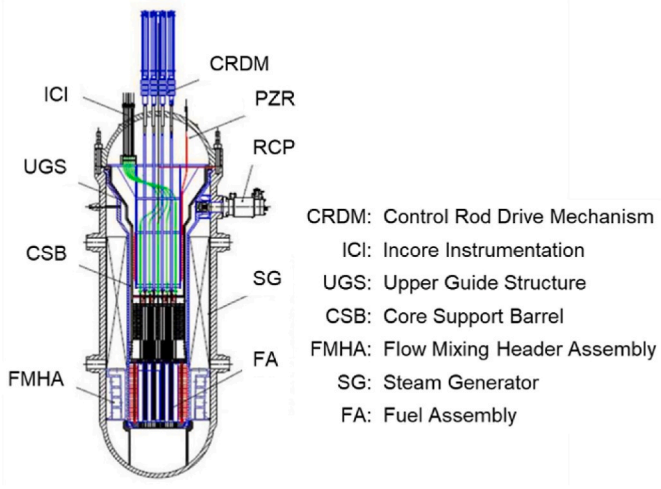

Fig. 3. RPV diagram of the SMART reactor.

The sequence of events in this analysis is as follows.

- Initial Event: A double-ended break occurs near the SIV in the steam line of SG1, simultaneously with a loss of offsite power.
- Rapid Pressure Decrease: Following the break in SG1, a quick reduction in secondary pressure occurs; the loss of offsite power leads to a coast down of all four main pumps.
- SCRAM Activation: SCRAM is initiated when the secondary pressure falls below 2 MPa.
- Valve Closures: The FWIVs, SIVs, and Turbine Stop Valve (TSV) close within 0.1 s after SCRAM.
- PRHRS Connection: The PRHRS IVs open, linking the PRHRS with the steam and feedwater lines in the same 0.1-s timeframe.
- Transient Duration: The total duration of the transient is set at 500 s.

It is noteworthy that the break in SG1 also impacts SG2 due to their connection via the PRHRS. In the TRACE model, SG1 and SG2 are represented as the third and fourth sectors of the VESSEL component, respectively.

4. The description of the models

This section delineates the models developed for TRACE, PARCS, and OpenFOAM, discussed in sequence.

4.1. The TRACE model

The TRACE SMART Model is structured around a 3D VESSEL component, serving to represent the RPV, as illustrated in Fig. 5. In this representation, a cylindrical discretization is employed, facilitating the inclusion of internal components such as the FMHA and the Flow Skirt, among others. Given that the SMART Reactor houses eight SGs within the RPV, positioned equidistantly from one another in the space between the Barrel and the external wall of the RPV, the RPV is discretized into eight azimuthal cells. To accurately model the intricate geometry of the four FMHAs, three cells are allocated in the radial direction (downcomer zone). Additionally, the model incorporates two additional radial cells to replicate the radial space housing the barrel along with the core. Axially, the RPV is divided into twenty-one cells for comprehensive representation.

In the upper section of the RPV resides the pressurizer, which is modeled as a pressurizer-type PIPE connected to the RPV via 8 pipes. Additionally, it is linked to safety relief valves, featuring opening and closing pressures of 18.7 MPa and 15.0 MPa, respectively. Adjacent to the pressurizer are the 4 centrifugal canned pumps, characterized by radial (outward) inlet suction and axial (downward) discharge. Positioned upstream to the SGs, these pumps are connected via pipes (tube bank cross-flow type) to the RPV and to heat structures, facilitating heat exchange with the secondary circuit. Highlighted in the figure are the BREAK and FILL components, which serve as interfaces for interaction with OpenFOAM.

The reactor core and the core bypass are represented using a vessel component with Cartesian coordinates, as depicted in Fig. 6. In this configuration, a discretization of none-by-nine cells is employed in a horizontal plane, complemented by twenty-two cells in the axial direction. This setup enables a one-to-one representation of the fifty-seven fuel elements of the SMART reactor, with some of the peripheral cells in the none-by-nine arrangement being axially blocked. Each fuel

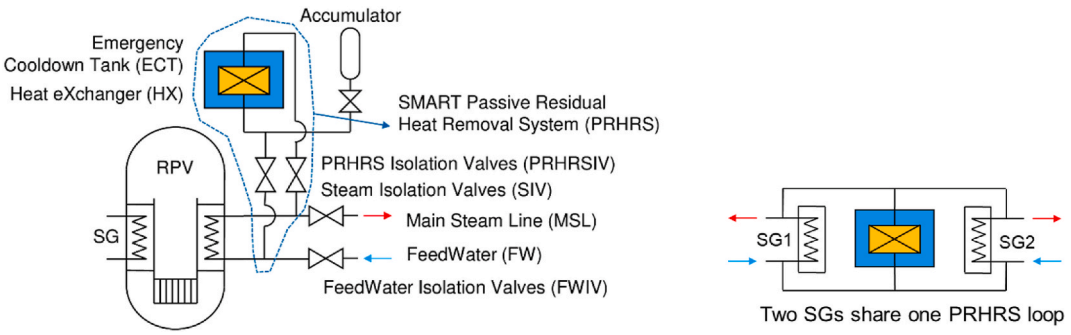

Fig. 4. The diagram of the SMART Passive Residual Heat Removal System (PRHRS) (left) and the configuration of one pair consisting of one PRHRS and two SGs (right).

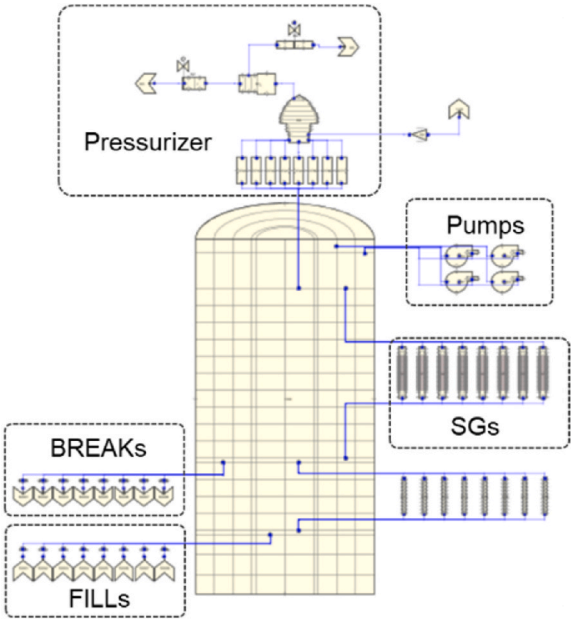

Fig. 5. The TRACE model of the SMART Reactor Pressure Vessel (RPV).

element is coupled to a heat structure to simulate core power. Notably, the first and last axial cells correspond to the lower and upper core grids, respectively, and thus no power is modeled in these regions.

The secondary side incorporates eight helical once-through SGs situated within the RPV, as depicted in Fig. 7. Each steam generator is equipped with its Feed Water (FW) system, FWIVs, and SIVs, which are activated in response to specific conditions, such as loss of FW, loss of offsite power, or steam line low pressure. In this simulation, the FW system is represented using TRACE's FILL components, which are connected to the FWIVs. Adjacent to the FWIVs are the helical tubes (SG pipes), linked to previously mentioned heat structures. These structures facilitate heat exchange with the primary side. The steam produced in these components is directed through the SIVs towards the turbine, represented as a break component, by passing through the MSL and the TSV.

The PRHRS represents another vital safety mechanism on the secondary side, designed to passively dissipate the core's residual heat during accidents, such as an SLB, as illustrated in Fig. 8. Upon closure of the FWIVs and SIVs, the steam generated in the SGs ascends to the HXs, where it condenses and returns to the SGs, thus establishing a natural circulation flow. The heat of condensation is extracted from the HXs by the ECT, which features an atmospheric vent modeled with a break component to maintain a fixed pressure. To prevent excessive pressure buildup, the system includes relief valves set to open at a pressure

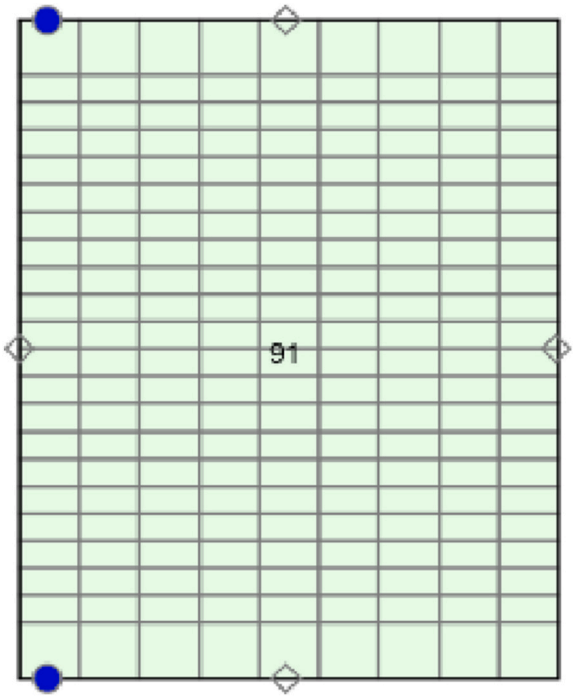

Fig. 6. The TRACE model of the SMART core.

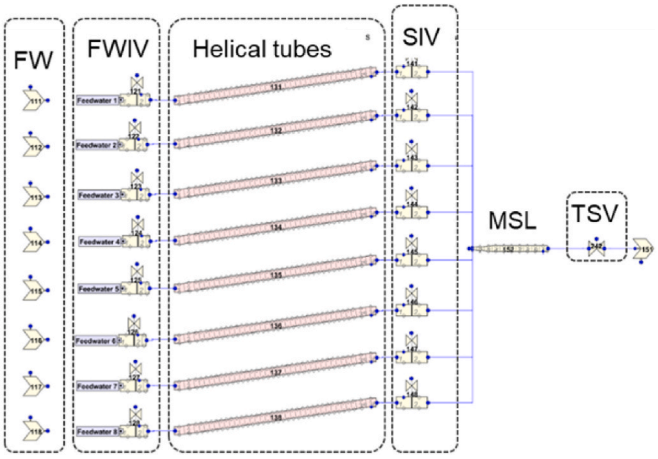

Fig. 7. The TRACE model of the SMART steam lines on the secondary side (FW-FeedWater, FWIV-FeedWater Isolation Valve, SIV-Steam Isolation Valve, MSL-Main Steam Line, TSV-Turbine Stopping Valve).

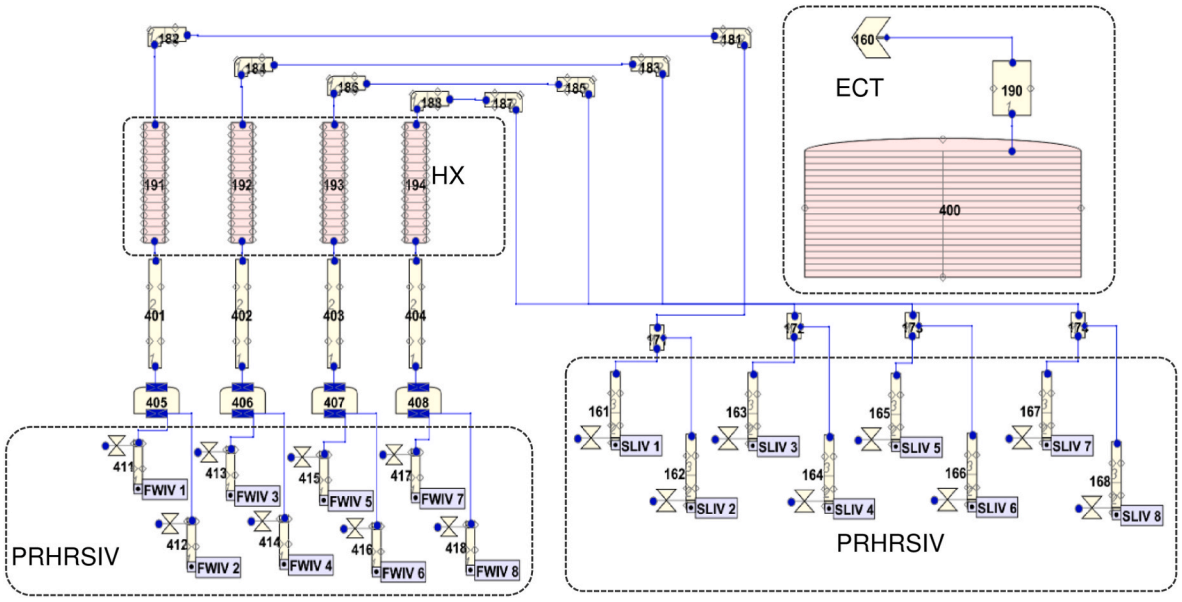

Fig. 8. The TRACE model of the SMART Passive Residual Hear Removal System (PRHRS) on the secondary side (PRHRSIV-PRHRS Isolation Valve, HX-Heat Exchanger, ECT-Emergency Cooling Tank).

similar to that of the pressurizer relief valves. This design aims to prevent the release of vapor into the atmosphere, especially considering the potential presence of fission products in the vapor.

4.2. The PARCS model

The PARCS core model for the SMART reactor, as seen from both top and 3D perspectives, is illustrated in Fig. 9. This model encapsulates the neutronic dynamics of the core through a discretized representation, consisting of fifty-seven radial nodes for the active core—one node per fuel assembly—and an additional forty nodes dedicated to the radial reflectors, each matching the dimensions of a fuel assembly (not shown in the figure). Vertically, the core is segmented into twenty-two layers, with the topmost and bottommost layers representing the axial reflectors (not shown in the figure), and the intervening twenty layers designated for the active core region. Each node within the PARCS model correlates directly to a corresponding node in the TRACE model within the Cartesian VESSEL component.

For each 3D node within the core, a set of nodal cross-section (XS) data is assigned, varying according to the TH feedback parameters and the specific material composition of the different types of fuel assemblies present in the core. These cross-sections were generated using the Monte Carlo neutronics code, Serpent (Leppänen et al., 2015). To accurately simulate the neutron behavior within the core, a nodal diffusion solver was employed, with a zero-flux boundary condition applied to the outermost radial and axial surfaces of the reactor core model, ensuring no neutron flux crosses these boundaries (the boundary of the reflectors).

4.3. The OpenFOAM model

Fig. 10 shows the CAD model utilized in OpenFOAM for the downcomer and lower plenum of the SMART reactor. Like any CFD simulation, this model incorporates design assumptions, geometry considerations, and assumed boundary conditions essential for its accurate representation. Notably, the model comprises three porosity sections, which effectively simulate the inlets and outlets of the FMHA along with the flow skirt. These porosity sections play a critical role in capturing the flow dynamics within the downcomer and lower plenum regions of the reactor.

In implementing this model, ANSYS was employed for mesh generation. The primary objective of meshing was to achieve a more stable

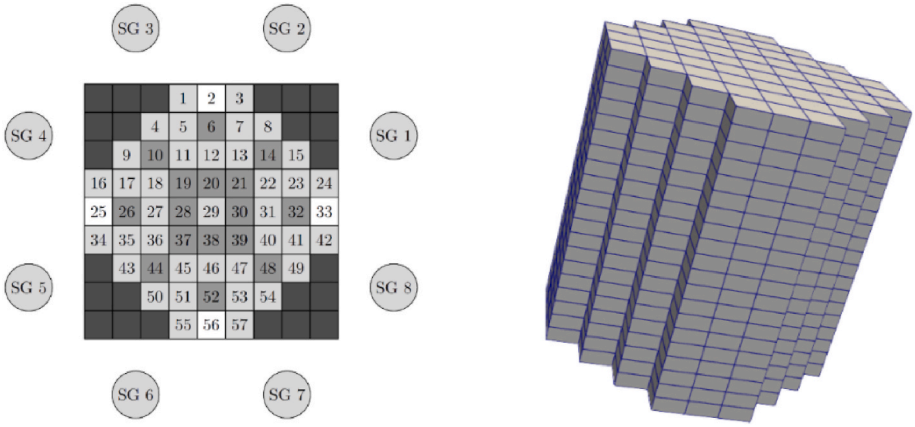

Fig. 9. Upper view (left) and 3D view (right) of core (SGs included in left figure). Dark gray - the blocked channels, Gray - the FAs with CR are extracted, Light gray - the FAs with CR are inserted, and White - the FAs without CR (left figure) (the reflectors are not shown in the 3D figure).

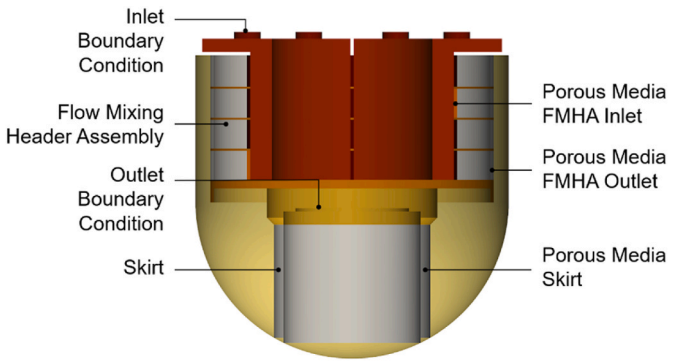

Fig. 10. Downcomer and lower plenum of the OpenFOAM model for the SMART reactor.

flow across all regions, ensuring acceptable y + values and minimal numerical residuals. This parameter holds significant importance for accurately simulating turbulence near the wall, as turbulence models possess restrictions on the y + value at the wall. For instance, the standard K-epsilon model necessitates a wall y + value ranging between approximately 30 and 300.

The initial step involved reviewing the topology, repairing any flaws, and ensuring geometry healing. This process not only ensures a correct and validated topology but also aids in comprehending the boundary conditions and model setups to facilitate volume splitting in a manner conducive to CFD meshing. With these considerations in mind, a mesh of high-quality meeting stringent criteria was generated, as depicted in Fig. 11. The mesh consists of approximately 40 million cells, predominantly comprising hexahedral elements with a low aspect ratio (average: 2.64) and exceptional characteristics in terms of distorted elements (low skewness average: 0.11) and high orthogonal quality (average: 0.944).

Subsequently, the mesh was successfully translated to OpenFOAM, which operates on a different mesh format. To utilize the obtained mesh within OpenFOAM, it was imperative to convert it into an ASCII Unix format. To accomplish this, the mesh needed to be reprocessed through a different meshing tool, ANSYS ICEM. Once this conversion process was completed, the mesh could be seamlessly imported into OpenFOAM, enabling the execution of its own CheckMesh routines to ensure mesh quality and integrity.

As previously mentioned, the coupling system has been parallelized to enhance the efficiency of OpenFOAM simulations. Leveraging the computational capabilities of the Horeka supercomputer at KIT, extensive testing was conducted to optimize the utilization of computational resources. Through these tests, it was determined that the most suitable configuration for this case entails the utilization of 1520 cores, distributed across 20 nodes with 76 cores each, coupled with a runtime allocation of 70 wall-hours.

5. The discussion of results

The subsequent sections provide an analysis of the Steady-State (SS) and Transient (TS) results derived from both the TRACE/PARCS and TRACE/PARCS/OpenFOAM models. In this context, the TRACE/PARCS solution is considered the reference against which the results from the coupled TRACE/PARCS/OpenFOAM model are compared and evaluated.

5.1. The steady-state result

Table 1 presents a comparison of the SS primary TH plant parameters computed by the models described in Section 4, alongside results computed by TRACE/PARCS, which serve as our reference. Notably, the differences between the coupled code and the reference (TRACE/PARCS) are minimal, with variations consistently below 0.15 % across all parameters. This close agreement underscores the accurate implementation of the coupled code and the meticulous construction of the models.

The data transfer between TRACE and OpenFOAM poses a significant computational challenge during both code development and simulations. It is imperative to thoroughly validate the accuracy of the fields transferred between TRACE and OpenFOAM bidirectionally. Fig. 12 illustrates the velocity magnitude field predicted by OpenFOAM within the coupling system for the SMART downcomer and lower plenum. The depiction of the SS coolant velocity distribution in the CFD model vividly portrays the flow trajectory of the coolant, with intricate vortex structures effectively captured.

Table 1
Steady-state results of Steam Line Break (SLB) accident for SMART reactor with TRACE/PARCS/OpenFOAM (TPO) compared with TRACE/PARCS (TP).

Parameter	TP (ref)	TPO	diff %
Primary pressure (MPa)	15.0	15.0	0.0
Core Power (MW)	330.0	330.0	0.0
Core inlet T (K)	567.36	566.62	0.13
Core outlet T (K)	594.76	594.15	0.10
Total mass flow rate (kg/s)	2090	2092	0.09
Core pressure drop (kPa)	35.1	35.1	0.0

Diff % = (TPO-TP)/TP * 100.

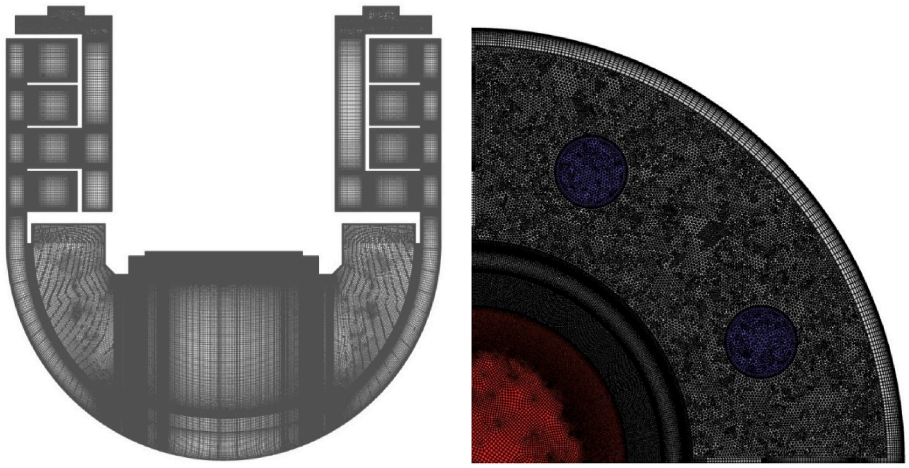

Fig. 11. Mesh details of the OpenFOAM model for the SMART reactor.

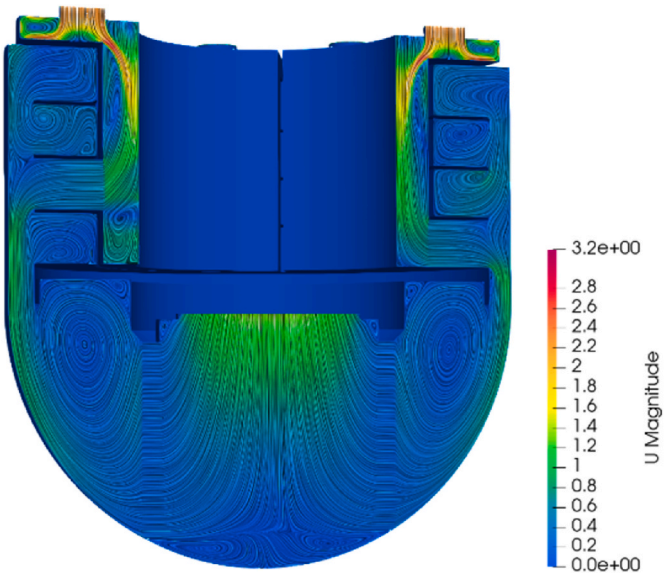

Fig. 12. Steady-State (SS) velocity magnitude predicted by OpenFOAM for SMART downcomer and lower plenum within the coupling system.

Regarding to the fields transferred from OpenFOAM to TRACE, Fig. 13 illustrates the distribution of mass flow rates at the core inlets (interfaces). It is observed that the mass flow rate at the core inlet interfaces rapidly converges to approximately 260 kg/s for each 1/8 core. This convergence signifies the robustness and effectiveness of our meticulously developed models and coupling codes.

5.2. The transient result

As stated earlier, the total simulation time for the transient scenario is 104 s, with the Steam Line Break (SLB) event initiating at 20 s within SG1. This results in a pressure drop in SG1, triggering a SCRAM once the pressure falls below 2 MPa. Concurrently, the pumps begin to coast down due to the loss of offsite power. Fig. 14 illustrates the evolution of power and pump speed over time, with results obtained from both the TRACE/PARCS/OpenFOAM and TRACE/PARCS simulations. In both figures, it is evident that the two solutions exhibit nearly identical curves, indicating strong agreement between the coupled and reference solutions. Moreover, the low power during this transient indicates that re-criticality and a return to power are not concerns in the SLB of the SMART reactor.

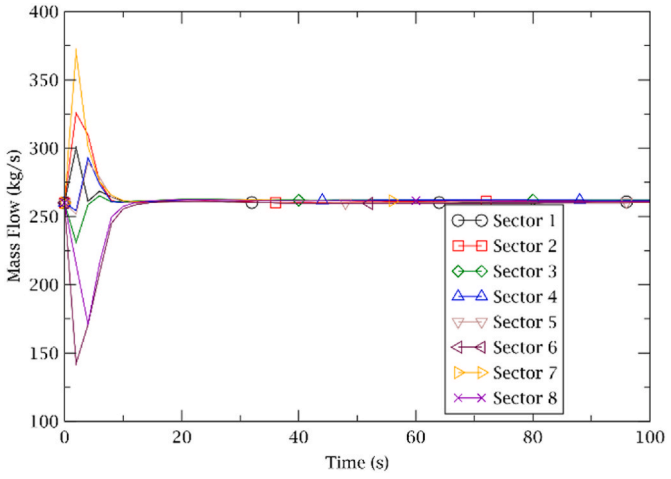

Fig. 13. The mass flow rate from OpenFOAM to TRACE at the core inlet (interfaces) during the Steady-State (SS) calculation for the SMART reactor.

Given that the SLB directly affects the SGs, it is imperative to initially investigate the phenomena occurring within the SGs. Fig. 15 displays the SG outlet temperatures obtained from both the TRACE/PARCS/OpenFOAM and TRACE/PARCS simulations. The legends in the figure correspond to the 8 sectors representing the 8 SGs, with SG1 and SG2 corresponding to sectors 3 and 4, respectively. In the results from TRACE/PARCS/OpenFOAM, SG1 initially experiences a decrease in temperature due to vaporization through the break. Subsequently, the temperature of SG1 increases as a result of the loss of heat sink (failure of PRHRS 1). Finally, the temperature of SG1 decreases thanks to its interaction with the other 6 SGs, which are continuously cooled down by PRHRS 2–4. Conversely, SG2 experiences an initial temperature increase immediately after the break due to rapid isolation from SG1 and the failure of PRHRS 1. Subsequently, its temperature decreases for the same reasons as SG1. In contrast, SG3-8 temperatures undergo only minor perturbations thanks to the functioning of PRHRS 2–4. The similar curves predicted by TRACE/PARCS further validate the performance of TRACE/PARCS/OpenFOAM, affirming the correct implementation of OpenFOAM within the multi-scale TH coupling system.

Fig. 16 illustrates the evolution of mass flow rates in the 8 SGs. Initially, the mass flow rate in SG1 experiences a slight increase due to the temperature decrease, which reduces flow resistance within SG1. Subsequently, it decreases as a result of the pump coasting down. Conversely, the mass flow rates in the other 7 SGs decrease over time due to the shutdown of the pumps. The disparity between SG1 and SG2 compared to SG3-8 is attributed to the higher temperature in SG1 and SG2, resulting in increased flow resistance and subsequently lower mass flow rates in these two SGs. However, the increasing tendency of mass flow rates in all SGs after the pumps are fully shut down indicates the initiation of natural circulation. Therefore, to a certain extent, it can be inferred that there is a successful transition from forced convection to natural flow.

In the investigation of TH conditions within the core, particularly focusing on core cooling, several notable observations arise from the comparisons between TRACE/PARCS and TRACE/PARCS/OpenFOAM solutions. In Fig. 17, depicting the mass flow rate through the core across all 8 sectors, similarities in decreasing and increasing tendencies before and after pump shutdown are evident between the two solutions. However, a significant difference emerges: TRACE/PARCS predicts a short-term reverse flow, while TRACE/PARCS/OpenFOAM consistently indicates an upward flow. This discrepancy becomes more pronounced when comparing the coolant mass flow rate, specifically in SG1, between the two solutions (Fig. 18, left). The reason could be the limitations of the code's standalone predicting the transition from forced flow to natural convection as well as the coupling of two complex TH domains. Further examination is warranted to understand this phenomenon in detail. Fig. 18 (right) presents the core inlet and outlet temperatures from both solutions. In TRACE/PARCS/OpenFOAM, the coolant temperature at the core inlet remains relatively stable, attributed to the functionality of the PRHRSs. Conversely, in TRACE/PARCS, the sudden temperature increase at the core inlet captures the occurrence of reverse flow.

The inclusion of CFD via OpenFOAM within our multi-physics and multi-scale TH system allows for a more detailed exploration of TH phenomena within its domain. Fig. 19 showcases the temperature field and velocity magnitude field predicted by OpenFOAM in the SMART reactor's downcomer and lower plenum at 100 s, which marks the end of the transient. Notably, OpenFOAM accurately captures the strong asymmetrical effects in both the temperature and velocity fields at the downcomer inlet. Furthermore, the flattened fields at the core inlet suggest effective mixing of the coolant flowing through the downcomer and lower plenum. However, despite these observations, uneven temperature distribution persists at the core inlet, indicating areas where further investigation may be warranted.

The utilization of OpenFOAM provides an opportunity to delve

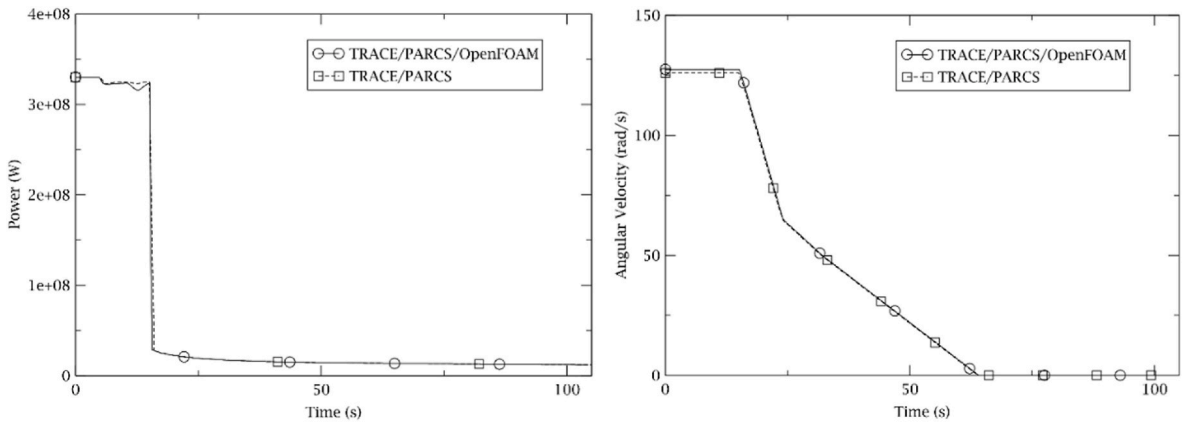

Fig. 14. The power evolution (left) and pump speed (right) over time during the Steam Line Break (SLB) transient for the SMART reactor.

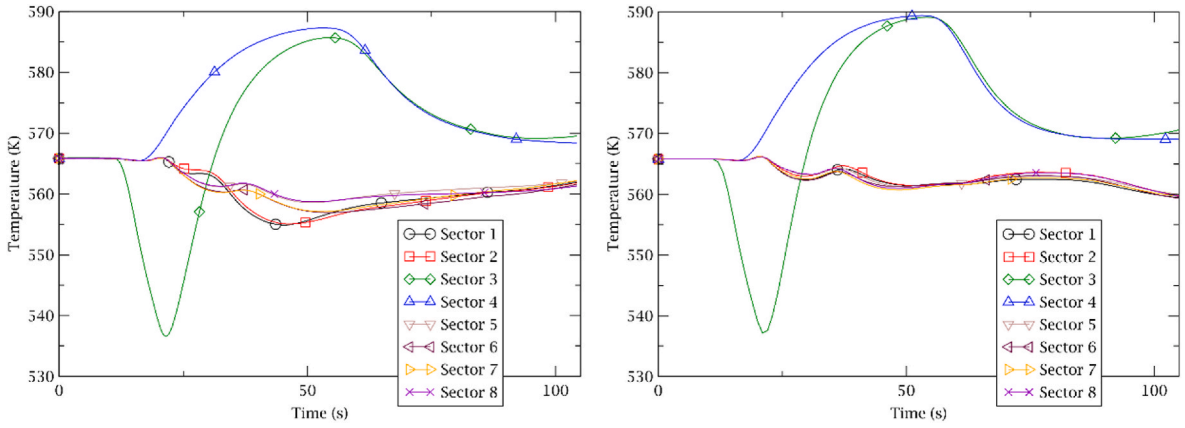

Fig. 15. The Steam Generator (SG) outlet temperature evolution of TRACE/PARCS/OpenFOAM (left) and TRACE/PARCS (right) over time during the Steam Line Break (SLB) transient for the SMART reactor.

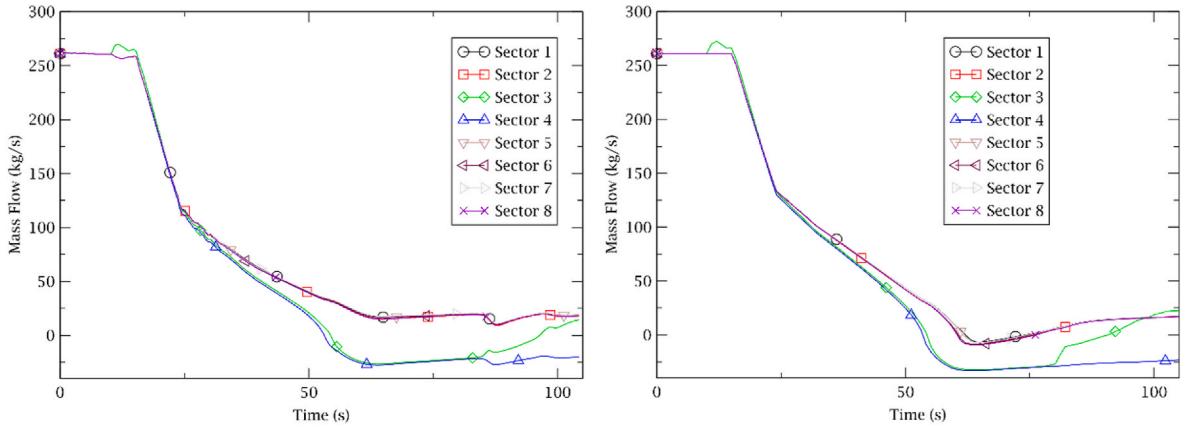

Fig. 16. The Steam Generator (SG) mass flow rate evolution of TRACE/PARCS/OpenFOAM (left) and TRACE/PARCS (right) over time during the Steam Line Break (SLB) transient for the SMART reactor.

deeper into the TH evolution details over time within the CFD domain. To illustrate the development of flow patterns along the flow path over time, we selected six time points for analysis, showcasing the coolant temperature distribution in the CFD domain. Fig. 20 presents six top views of the coolant temperature distribution, representing time points at 10s, 25s, 40s, 65s, 80s, and 100s. The first two plots on the left are derived from previous figures, showcasing the SG outlet temperature and mass flow rate, respectively. These global maps offer a clear depiction of the CFD fields.

At 10s, before the initiation of the SLB, the coolant temperature appears homogenized. Subsequently, at 25s, the portion relevant to Sector 3 experiences cooling due to evaporation in SG1, while the portion relevant to Sector 4 begins to heat up. By 40s, the temperature in SG2 and SG1 is approaching its peak value, with SG2 exhibiting higher temperatures than SG1. From 65s to 100s, the coolant temperature in SG1 and SG2 gradually decreases, attributable to the operation of

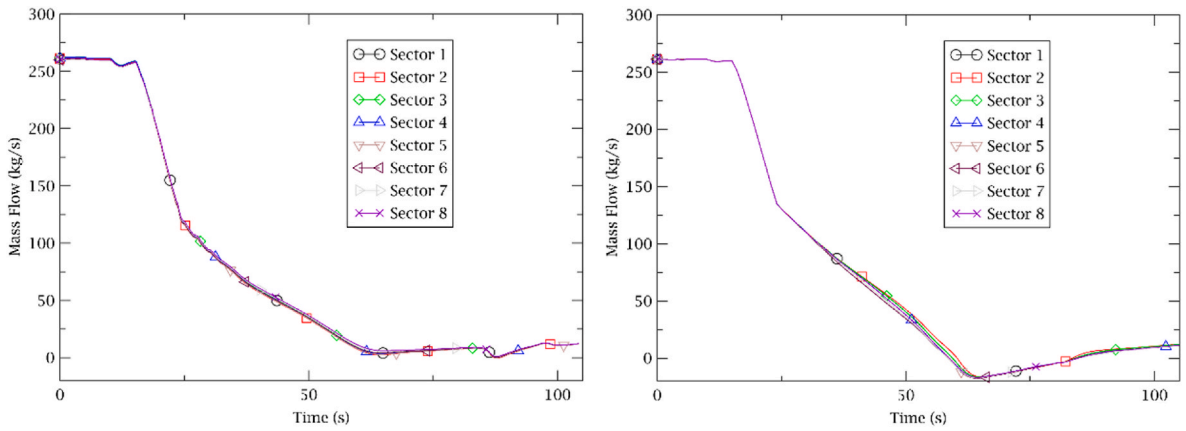

Fig. 17. The core mass flow rate evolution of TRACE/PARCS/OpenFOAM (left) and TRACE/PARCS (right) over time during the Steam Line Break (SLB) transient for the SMART reactor.

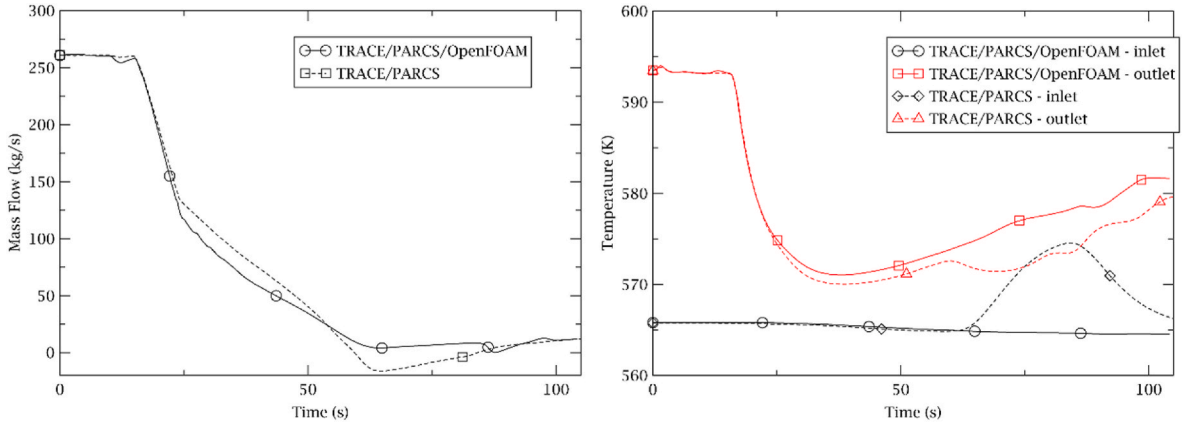

Fig. 18. The 1/8 core mass flow rate evolution (left) and the core inlet/outlet temperature (right) of TRACE/PARCS/OpenFOAM and TRACE/PARCS over time during the Steam Line Break (SLB) transient for the SMART reactor.

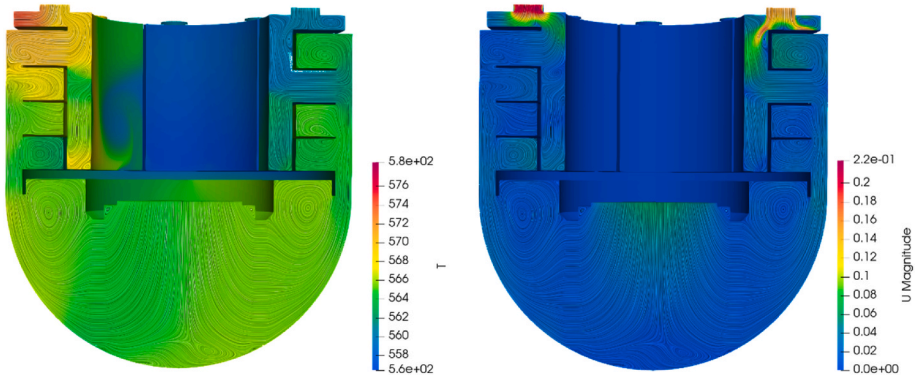

Fig. 19. The coolant temperature (left) and velocity magnitude (right) predicted by OpenFOAM for SMART downcomer and lower plenum at the end of the transient (TS).

PRHRS 2–4. Throughout the transient, the regions relevant to SG 3–8 show minimal temperature variation.

To further elucidate the flow dynamics, the CFD domains are sectioned axially at an angle of minus 45° in the xy coordinates, as depicted in Fig. 21. The correspondence of coolant temperatures at the CFD inlets between Figs. 20 and 21 is readily apparent. Given that the coolant temperature varies most notably in sectors 3 and 4, while the other 6 sectors exhibit minimal change, our focus is directed toward understanding the evolution of flow conditions in sectors 3 and 4.

Between 10s and approximately 30s, a significant influx of cooler coolant is observed entering the downcomer from the position of sector 3 (upper left of the CFD domain in Fig. 20, reflected in the slice at 25s in Fig. 21). while sector 4 experiences a slight increase in coolant temperature. Overall, sectors 3 and 4 exhibit an influx of cooler coolant during this period. Subsequently, the coolant in this region begins to warm up. However, as the mass flow rate decreases, the cooler fluid continues to exit the CFD domain, interacting with the warmer fluid entering thereafter and with fluid from other sectors. This interaction

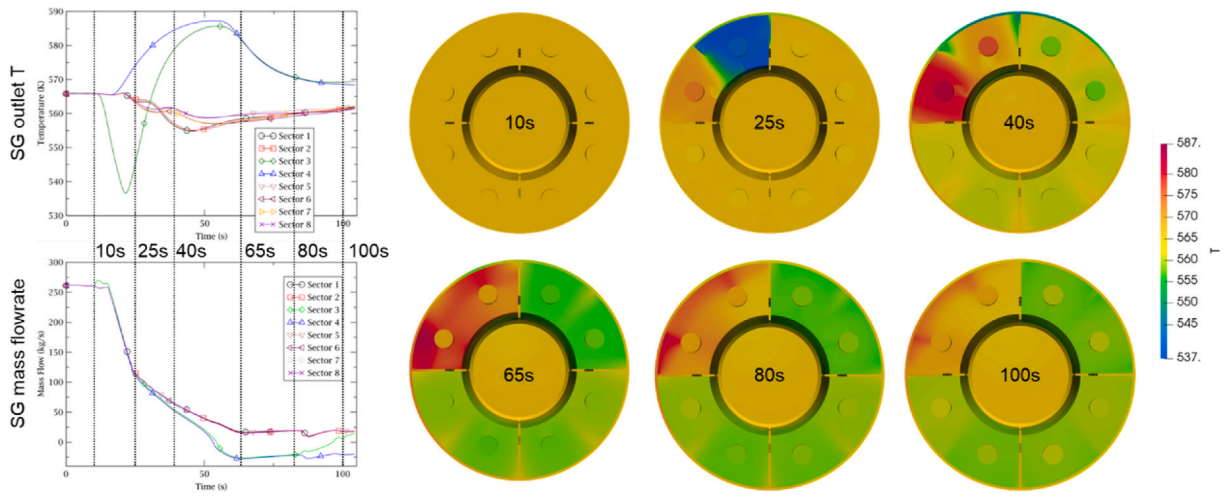

Fig. 20. The coolant temperature evolution at the CFD domain inlet during the Steam Line Break (SLB) in the SMART reactor.

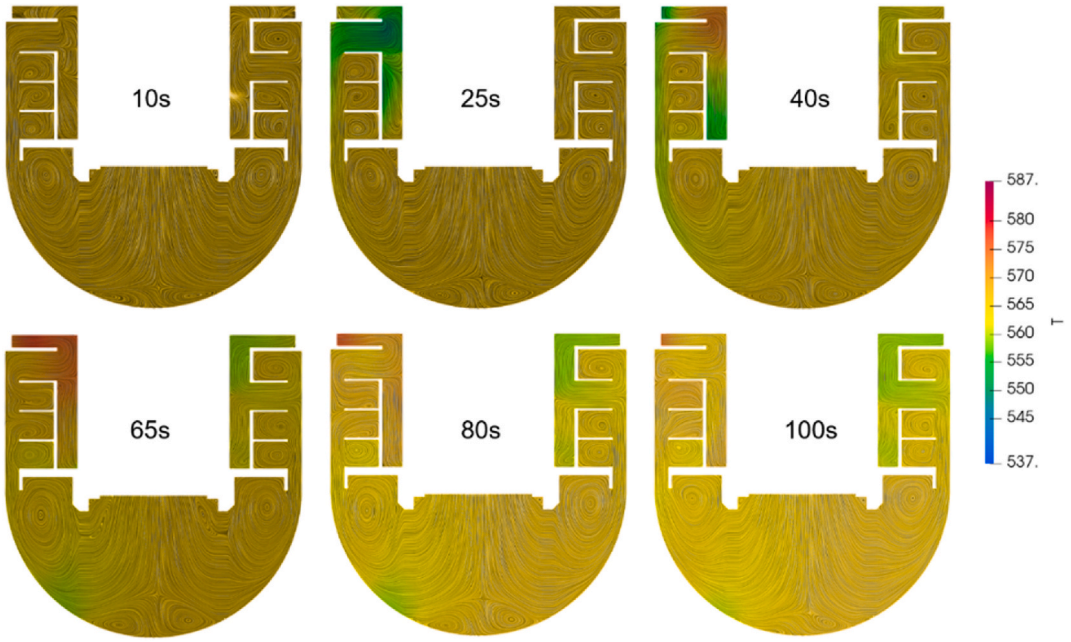

Fig. 21. The coolant temperature evolution on a slice of the CFD domain during the Steam Line Break (SLB) in the SMART reactor.

facilitates the development of flow patterns in the downcomer and lower plenum (as evidenced by the slices at 40s, 65s, and 80s in Fig. 21). An evident cooler region is discernible at the lower left of the lower plenum, indicating a relatively stagnant area which may be attributed to the presence of the flow skirt in the lower plenum.

6. Conclusions

The paper conducts a safety analysis of the Steam Line Break (SLB) accident for the SMART Small Modular Reactor (SMR) utilizing the newly-developed multi-physics multi-scale coupled code TRACE/PARCS/OpenFOAM at the Karlsruhe Institute of Technology (KIT). This study falls within the framework of the European McSafer project. The coupled code adeptly captures several key global phenomena during the SLB accident, including the sudden and significant pressure drop in the steam generators, the subsequent power decrease due to SCRAM, the reduction in core mass flow rate resulting from the coasting down of the main pumps, and the increase in primary coolant temperature due to residual core heat, among others. Furthermore, the detailed flow characteristics provided by the OpenFOAM analysis enable an in-depth examination of flow pattern development in the downcomer and lower plenum. The mixing behavior of hotter and cooler coolant at the downcomer inlet (CFD inlet) and the core inlet (CFD outlet) is accurately captured. Notably, the strong asymmetrical distribution of coolant temperature at the CFD inlet is effectively flattened at the CFD outlet, demonstrating the efficacy of the flow mixer in the downcomer and the flow skirt in the lower plenum. The coupled code successfully predicts the establishment of natural circulation in the primary circuit and the activation of the Passive Residual Heat Removal System (PRHRS), ultimately affirming the inherent safety features of the SMART reactor.

CRediT authorship contribution statement

Kanglong Zhang: Writing – original draft, Software, Methodology, Formal analysis. **Victor Hugo Sanchez-Espinoza:** Writing – review & editing, Project administration, Funding acquisition, Conceptualization.

Declaration of competing interest

The authors declare that they have no known competing financial interests or personal relationships that could have appeared to influence the work reported in this paper.

Acknowledgment

The authors wish to acknowledge the support of the EU McSafer project Nr. 945063 which was coordinated by the Karlsruhe Institute of Technology (KIT).

Data availability

The authors do not have permission to share data.

References

Bajorek, S.M., et al., 2015. Development, validation and assessment of the TRACE thermal-hydraulics system code. In: 16th International Topical Meeting on Nuclear Reactor Thermal Hydraulics (NURETH-16), pp. 8265–8278. Chicago, IL.

Calleja, M., Sanchez, V., Jimenez, J., Imke, U., Stieglitz, R., Macián, R., 2014. Coupling of COBAYA3/SUBCHANFLOW inside the NURESIM platform and validation using selected benchmarks. Ann. Nucl. Energy 71, 145–158. https://doi.org/10.1016/j.anucene.2014.03.036.

Chung, Y.-J., Kim, H.-R., Chun, J.-H., Kim, S.-H., Bae, K.-H., 2015. Strength assessment of SMART design against anticipated transient without scram. Prog. Nucl. Energy 85, 617–623. https://doi.org/10.1016/j.pnucene.2015.08.005.

Downar, T., Xu, Y., Seker, V., 2012. Theory Manual for the PARCS Kinetics Core Simulator Module.

Hugo Sanchez-Espinoza, V., Zhang, K., Campos Muñoz, A., Böttcher, M., 2023. KIT Multi-scale thermal–hydraulic coupling methods for improved simulation of nuclear power plants. Nucl. Eng. Des. 405, 112218. https://doi.org/10.1016/j.nucengdes.2023.112218.

International Atomic Energy Agency, 1997. Status of Advanced Light Water Cooled Reactor Designs 1996. IAEA-TECDOC-968, Vienna, Austria [Online]. Available: http://www-pub.iaea.org/MTCD/Publications/PDF/te_968_prn.pdf. (Accessed 15 December 2021).

International Atomic Energy Agency, 2021. "Technology Roadmap for Small Modular Reactor Deployment, IAEA Nuclear Energy Series No. NR-T-1.18," Vienna, Austria [Online]. Available: https://www-pub.iaea.org/MTCD/Publications/PDF/PUB1944_web.pdf. (Accessed 22 December 2021).

Kamalpour, S., Khalafi, H., 2021. SMART reactor core design optimization based on FCM fuel. Nucl. Eng. Des. 372 (Feb). https://doi.org/10.1016/j.nucengdes.2020.110970.

Leppänen, J., Pusa, M., Viitanen, T., Valtavirta, V., Kaltiaisenaho, T., 2015. The Serpent Monte Carlo code: status, development and applications in 2013. Ann. Nucl. Energy 82, 142–150. https://doi.org/10.1016/j.anucene.2014.08.024.

Liu, L., et al., 2024. An innovational Jacobian-split Newton-Krylov method combining the advantages of the Jacobian-free Newton-Krylov method and the finite difference Jacobian-based Newton-Krylov method. Nucl. Sci. Eng. 198 (10), 1911–1934. https://doi.org/10.1080/00295639.2023.2284447.

OpenFOAM Foundation. OpenFOAM homepage [Online]. Available: https://openfoam.org/. (Accessed 13 March 2024).

Sadegh-Noedoost, A., Faghihi, F., Fakhraei, A., Amin-Mozafari, M., 2020. Investigations of the fresh-core cycle-length and the average fuel depletion analysis of the NuScale core. Ann. Nucl. Energy 136 (Feb). https://doi.org/10.1016/j.anucene.2019.106995.

SALOME Platform. MEDCoupling developers' guide: the ICoCo API [Online]. Available: https://docs.salome-platform.org/latest/dev/MEDCoupling/developer/icoco.html. (Accessed 21 March 2024).

SALOME Platform. MEDCoupling developer's guide [Online]. Available: http://docs.salome-platform.org/latest/dev/MEDCoupling/developer/index.html. (Accessed 21 March 2022).

Sanchez-Espinoza, V.H., et al., 2021. The H2020 McSafer project: main goals, technical work program, and status. Energies 14 (19). https://doi.org/10.3390/en14196348.

Sanchez-Espinoza, V.H., et al., 2023. KIT reactor safety research for LWRs: research lines, numerical tools, and prospects. Nucl. Eng. Des. 414, 112573. https://doi.org/10.1016/j.nucengdes.2023.112573.

Tashakor, S., Zarifi, E., Naminazari, M., 2017. Neutronic simulation of CAREM-25 Small modular reactor. Prog. Nucl. Energy 99, 185–195. https://doi.org/10.1016/j.pnucene.2017.05.016.

Watson, J.K., Ivanov, K.N., 2012. Demonstration of implicit coupling of TRACE/PARCS using simplified one-dimensional problems. Nucl. Technol. 180 (2), 174–190. https://doi.org/10.13182/NT12-A14632.

Zhang, K., 2020. The multiscale thermal-hydraulic simulation for nuclear reactors: a classification of the coupling approaches and a review of the coupled codes. Int. J. Energy Res. 44 (5), 3295–3315. https://doi.org/10.1002/er.5111.

Zhang, K., Sanchez-Espinoza, V., 2023. Multi-scale coupling of TRACE and SubChanFlow (SCF) in the SALOME platform using the domain decomposition (DD) method and a conservative data transfer approach. In: 20th International Topical Meeting on Nuclear Reactor Thermal Hydraulics (NURETH-20). American Nuclear Society, Illinois, pp. 1066–1075. https://doi.org/10.13182/NURETH20-40266.

Zhang, H., Guo, J., Lu, J., Li, F., Xu, Y., Downar, T.J., 2018. An assessment of coupling algorithms in HTR simulator TINTE. Nucl. Sci. Eng. 190 (3), 287–309. https://doi.org/10.1080/00295639.2018.1442061.

Zhang, K., Zhang, X., Sanchez-Espinoza, V., Stieglitz, R., 2020a. Development of the coupled code – TRACE/TrioCFD based on ICoCo for simulation of nuclear power systems and its validation against the VVER-1000 coolant-mixing benchmark. Nucl. Eng. Des. 362, 110602. https://doi.org/10.1016/j.nucengdes.2020.110602.

Zhang, X., Zhang, K., Sanchez-Espinoza, V.H., Chen, H., 2020b. Multi-scale coupling of CFD code and sub-channel code based on a generic coupling architecture. Ann. Nucl. Energy 141, 107353. https://doi.org/10.1016/j.anucene.2020.107353.

Zhang, K., Muñoz, A.C., Sanchez-Espinoza, V.H., 2021. Development and verification of the coupled thermal–hydraulic code – TRACE/SCF based on the ICoCo interface and the SALOME platform. Ann. Nucl. Energy 155, 108169. https://doi.org/10.1016/j.anucene.2021.108169.